High-resolution Computed Tomography (microCT) Technique for Capturing Soft Tissue Intervertebral Disc Changes After Repeated Loading

Concetta F. Morino, Shea T. Middleton, Elizabeth D. Dimbath, Jason R. Kait,
Jason F. Luck, Cameron R. Dale Bass

Abstract There is a critical need to visualise intervertebral disc (IVD) changes prior to clinically detectable injuries, as most people with low back pain have no detectable pathology, resulting in generalised and often ineffective treatment options.

Nine porcine IVDs subjected to repeated loading and one control were imaged prior to and after loading with high-resolution microCT. For pre-test and post-test imaging, frozen specimens were positioned in an insulated container and microCT images were acquired using a 0.125 mm copper filter, 708 ms exposure time, 90–110 kV beam energy, and 700–800 μA beam current. Specimens were loaded under repeated flexion-compression at exposures below endplate injury risk. The control specimen was not loaded but exposed to identical environmental conditions.

The novel microCT imaging technique resolved soft tissue components, such as individual lamellae in the annulus fibrosus (AF) and non-water constituents of the nucleus pulposus (NP), at resolutions of 34.9–45.0 voxels/mm. With this enhanced image quality, post-test images revealed that the three test specimens loaded near the endplate injury threshold exhibited annulus separation and blurred NP-AF boundaries compared to pre-test images.

The current study established a useful, non-destructive methodology for imaging IVD tissue and captured pre-injury IVD morphology.

Keywords Annulus fibrosus separation, Disc injury, MicroCT, Non-specific low back pain, Soft tissue imaging.

I. INTRODUCTION

Most people will experience low back pain (LBP) at some point in their lives, yet an overwhelming majority of LBP patients, estimated at around 90%, have non-specific LBP, meaning that no specific pathology (i.e. fracture, stenosis) could be confirmed [1-2]. One reason most patients cannot receive a specific LBP diagnosis is attributed to the limited capabilities of current diagnostic tools. It has been demonstrated that current clinical imaging, including x-ray, computed tomography (CT), and magnetic resonance imaging (MRI), does not improve patient outcomes [3-4] and clinicians have been advised in more recent years to avoid ordering clinical imaging for their patients who do not exhibit specific red flags for the few known diagnoses (i.e. recent trauma) because of the low clinical benefit, high cost to the patient, and unnecessary radiation exposure [4-5]. However, the etiology of injuries contributing to LBP remains still largely unknown, further contributing to the difficulty of diagnosis.

Degradation of the intervertebral disc (IVD) is a known contributor to LBP, such as in cases of degenerative disc disease or disc herniations. The IVD, comprised of the gel-like hydrated nucleus pulposus (NP) and fiber-reinforced annulus fibrosus (AF), plays a critical role in the mechanical functions of the spine, acting as a shock-absorber and enabling range of motion for rotation, bending, and twisting [6]. In healthy discs, the AF is comprised of highly organised collagen fibers that form the concentric lamellae, bound together with elastin [7-8]. Under load, the AF constrains the NP and limits large outflow of fluid from the disc [9]. Any breakdown in these constituents can greatly alter the biomechanical function and load-bearing capacity of the spinal unit [9-12]. Healthy discs are mostly aneural, with some innervation on the outer annulus fibers, but recent studies have

C. F. Morino (e-mail: concettamorino@gmail.com; tel: (980) 221-8111) is a PhD graduate in mechanical engineering, E. Dimbath is a PhD graduate in biomedical engineering, S. T. Middleton is a PhD student in biomedical engineering, J. R. Kait is a research engineer in the Department of Biomedical Engineering, and J. F. Luck is an Assistant Research Professor in the Department of Biomedical Engineering, all at Duke University, USA. C. R. D. Bass is a Professor in the Department of Biomedical Engineering at Wayne State University, USA.

shown degenerated discs to have an increased number and density of nerve fibers that extend deeper into the AF and sometimes into the NP [13-15]. With increased neural presence comes an increased likelihood of pain in patients with damaged IVD constituents. Microscale, low-level damage to the IVD, preceding detectable bulges or herniations, has the potential to be a source of pain in many suffering from non-specific LBP.

Clinical imaging for LBP is limited and mostly unsuccessful at capturing pain-inducing injury, so many studies have aimed to capture IVD tissue damage experimentally [e.g. 16-18]. Histology techniques can show microscale tissue damage, but this technique is inherently destructive. For non-destructive imaging, x-ray, CT, and MRI are commonly employed for imaging biological tissue. Generally, x-ray and CT imaging are utilised for imaging denser materials like bone, while MRI is commonly utilised for soft tissue imaging. Standard MRI techniques can discern NP from AF, but the image resolution in these studies is significantly lower with respect to microCT, which is the modality employed in the current study. Recent IVD MRI studies report spatial resolutions of approximately 3.2–3.6 pixels/mm and 1.2–1.5 mm slice thickness [e.g. 19-20] compared to Morino *et al.* [21] which used microCT, with spatial resolutions of approximately 12–13 voxels/mm in all directions (0.08–0.09 mm slice thickness).

Micro-computed tomography, or microCT, is a relatively new, increasingly accessible, high-resolution imaging modality that uses x-rays to construct three-dimensional images of objects with resolutions down to the micron [22]. Because soft tissues have low x-ray absorption, soft tissue components typically have low contrast in microCT images, making tissue components difficult to discern from one another. While contrast agents can improve the image, it is unclear how these contrasting agents and associated tissue fixation procedures alter the tissue properties [22-23]. Recently, in our study investigating incipient lumbar endplate injury, Morino *et al.* used microCT imaging to capture lumbar endplates but incidentally also produced imaging of the IVD with discernible soft tissue components [21]. The results from [21] led to the primary hypothesis for the current study, that microCT imaging can be utilised to visualise soft tissue components of the IVD, such as individual annulus layers and non-water NP components, at high resolutions without the use of a contrast agent. The primary objective of this study was to develop and evaluate high-resolution microCT imaging techniques for improved visualisation of IVD soft tissue. The secondary objective was to apply this novel high-resolution imaging technique to capture tissue changes in the porcine IVD components after repeated loading exposures prior to endplate failure.

II. METHODS

Full cadaver lumbar spines (from the last thoracic vertebral body, TX, to the last lumbar vertebral body, L6 in pig) were extracted from nine young adult Yorkshire pigs (average mass 62 ± 17 kg) and separated into functional spinal units (FSUs). Cadaver porcine tissue was procured from post-mortem specimens of the Duke Division of Laboratory Animal Resources. FSUs were comprised of two adjacent vertebral bodies, an intervertebral disc, and associated ligaments, with most overlaying musculature and fat removed. FSUs vertebral body levels ranged from TX-L1 to L5-L6. After FSU separation, specimens were kept frozen at -20°C until test preparation. Specimens were refrozen following experimental testing.

High-Resolution Imaging

It was essential to keep specimens frozen to minimise specimen movement during scanning for this methodology, as any specimen movement would greatly degrade the final image quality due to the small voxel size and long frame exposure time. To secure the specimen in an optimal position, with the transverse plane of the IVD parallel to the base of the microCT stage, a customisable clay mounting fixture was shaped to the inferior end of each FSU. The mounting fixture was made from Roma plastilina #1 modelling clay, which was rigid enough to hold the weight of the specimen without deforming, but pliable enough to mould around each individual FSU inferior surface curvature. To prevent thawing, and thus subsequent movement, the mounting fixture and specimen were enclosed in an insulated cooler (Coleman© 1-Gallon Water Jug) with a small piece of dry ice (CO_2) placed above the specimen, approximately the size of one vertebral body. The flip-top spout for this insulator allowed for releasing evaporated carbon dioxide gas from the dry ice after the lid was sealed (Fig. 1).

The cooler was placed in the centre of the microCT stage after sample fixation (Nikon Metrology Inc., Model XTH 225 ST, Brighton, MI). A copper filter (0.125 mm) was placed in front of the detector, between the detector and sample. X-rays were turned on when positioning the sample. Ren *et al.* [24] demonstrated that copper filtration improves microCT image quality of low-density bone, lung tissue, and muscle tissue by increasing the contrast-to-noise ratio. The region of interest (ROI) for images in this study included the entire IVD and adjacent endplates. To maximise the ROI in the frame, posterior elements, lateral elements, and distal ends of vertebral

bodies (VBs) were not fully included in the scan. For the specimens in this test series, voxel sizes ranged from 22.2 µm to 28.7 µm, with corresponding spatial resolutions ranging from 34.8 voxels/mm to 45.0 voxels/mm. Resolution and voxel size were dictated by how close the specimen was to the detector.

The general image settings used for this study are shown in Table I. The settings for these scans result in approximately 94-minute acquisition time. The ultimate goal for each scan was to maximise the power while avoiding overexposing the voxels (white target below 60,000). For each scan, the starting voltage was 90 kV and starting current was 800 µA. If the voxels were still below the white target, the voltage was increased by 1 kV until the white target reached approximately 58,000. If the starting settings of 90kV and 800 µA were already overexposed, the current was reduced to 700 µA, and again, the voltage was increased by 1 kV until the white target reached approximately 58,000. This process resulted in slightly different voltages and currents between scans but maximal power for each individual scanned specimen while avoiding overexposed voxels. Generally, the maximum power achievable without overexposure was dependent on the filament and age of the filament at the time of the scan which inherently varies between scans. Pre-test and post-test scan settings for the same specimen were not necessarily the same. No beam hardening or noise reduction were applied to the images.

TABLE I
GENERAL MICROCT SETTINGS

Shading Correction Settings		*Acquisition Settings*	
Frames to average	300	Exposure time	708 ms
Number of images	3	Gain	24.0 dB
White target	60,000	Beam energy	90-110 kV
		Beam current	700-800 µA
		Projections	2,000
		Frames per projection	4
		Filter	Copper
		Filter size	0.125 mm

Cross-sectional areas of the interior endplates (inferior endplate of superior VB, superior endplate of inferior VB) and endplate-to-endplate (EP-EP) heights were measured using pre-test microCT images. Endplate-to-endplate height in this study was used for engineering strain calculations and defined as the distance from the bottom of the superior vertebral body to the top of the inferior vertebral body (Fig. 2). This distance varies across the surface of the endplate, so the EP-EP height is an average value across the endplate. After testing, all experimental and control specimens were imaged again using the same procedure and general microCT settings.

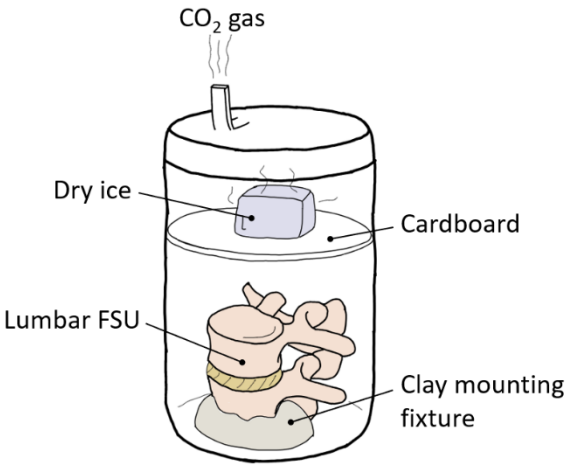

Fig. 1. Schematic for sample fixation. Specimen is held upright with clay mounting fixture. Dry ice is supported by a round cardboard piece. Top spout allows for CO_2 gas release.

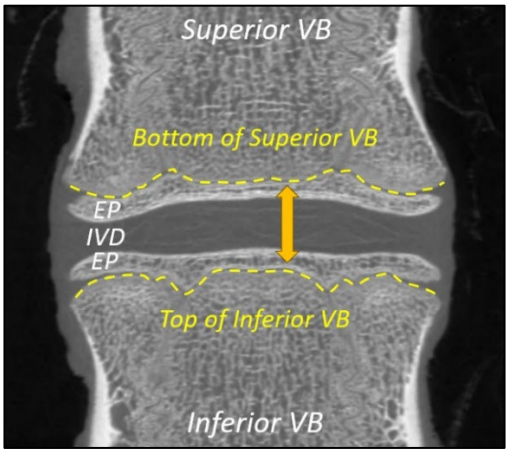

Fig. 2. EP-EP height measured from the bottom of the superior VB to the top of the inferior VB, as indicated by the yellow dotted lines. Measurements were taken throughout the FSU from anterior to posterior slices and then averaged for the resulting average initial EP-EP height.

Mechanical loading inherently changes the specimen from its pre-test form, and the specimens were manually positioned for scanning, therefore it was not possible in this study to obtain identical pre- and post-test slices for comparison. To obtain comparable mid-disc slices from before and after testing, the specimen was first rotated

(using 3D Slicer software 5.2.2) to position the transverse plane of the IVD to be horizontal. In the coronal view, the sagittal plane slice was positioned at the midpoint of the leftmost and rightmost disc tissue. In the sagittal view, the coronal plane slice was positioned near the thickest part of the disc /the thinnest part of the endplate. The axial plane slice was positioned near the midpoint of the thickest part of the disc in the sagittal view. Figure 3 shows all three views and slice location for the control specimen.

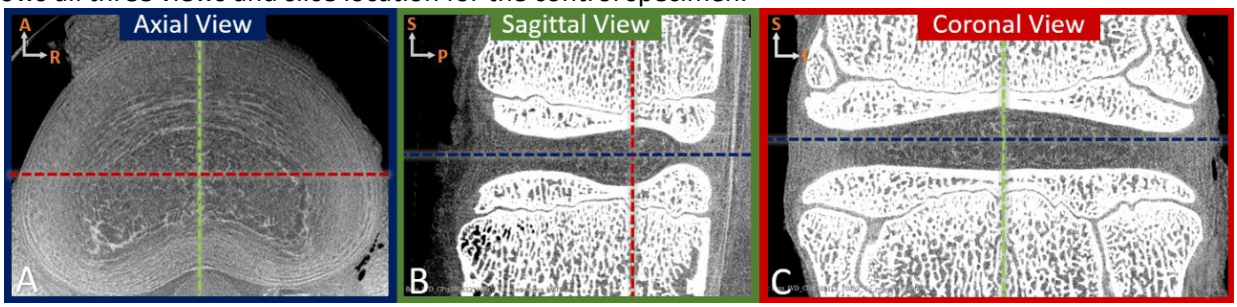

Fig. 3. Pre-test and post-test images matching process for Control: (A) axial view showing sagittal (green dotted) and coronal (red dotted) planes; (B) sagittal view showing axial (blue dotted) and coronal planes; and (C) coronal view showing axial and sagittal planes. Orientation axes denote anatomical anterior 'A', posterior 'P', left 'L', right 'R', and superior 'S' directions.

Experimental Testing

Specimen preparation and the loading profile/experimental testing set-up used in this study were identical to a prior combined flexion-compression loading study in Morino *et al.* [21]. In that study, human and porcine FSUs were loaded in repeated combined flexion-compression in a biaxial test fixture until endplate failure to establish an endplate fracture risk for human and porcine lumbar spine in repeated loading. In this study, the 50% injury risk curve from [21] was used to inform the loading stress and duration to load the current specimens just below the established endplate injury risk exposure.

After acquiring pre-test images, specimens were kept frozen until preparation. One day before test preparation, specimens were thawed in a refrigerator (4°C). The vertebral bodies were fixed into aluminum cups by drilling screws and wires into the distal ends of the vertebral bodies, which were then covered in polymethyl methacrylate (PMMA), and fixed into the cups using urethane casting resin (R1 Fast Cast® #891, Goldenwest Mfg, Inc. Grass Valley, CA). This fixation process is covered in greater detail in [21].

Prior to loading, control and test specimens were positioned in the biaxial test fixture and subjected to heat and humidity until temperature reached 37°C and humidity was over 90%. The general loading profile applied to the specimens was identical to [21], which was originally modelled after real-world loading exposures measured in high-speed boat occupants [21][25]. The loading profile consisted of sinusoidal compression at 1 Hz, applied to the inferior end of the specimen, while the superior end was subject to an offset 1 Hz ramp flexion, starting at 80% of the compressive peak. This loading simulates repeated underbody loading, followed by the inertial response of upper-body flexion forward.

A range of loading exposures below the 50% endplate fracture threshold were applied to test specimens. A peak compressive stress, 2.75 MPa, was consistent for all tests, and loading duration depended on the intended final engineering strain (displacement over initial EP-EP height), resulting in a range of applied exposures. Peak compressive load was calculated from the peak compressive stress (2.75 MPa) multiplied by the measured average endplate cross-sectional area between the two interior FSU endplates. The minimum compressive load, 76 N, represented an average torso load, which is approximately 200 N for human, scaled to pig by lumbar endplate area [21]. Specific characteristics for each specimen and loading parameters are provided with results in Table II. The control specimen in this study was imaged and prepared identically to experimental specimens. The control was fixed in the same biaxial test fixture with no applied loading and exposed to the same temperature and humidity environmental conditions for the same duration as Test 1, the longest exposure test.

III. RESULTS

Improving Image Resolution and Quality

The primary objective was to develop a methodology to improve the visualisation of individual soft tissue components of the IVD using non-invasive, non-destructive microCT, a technology typically used for imaging denser constituents, such as bone. Results from [21] indicated that microCT could be used in a non-destructive manner to image microscale soft tissue constituents. Because microCT has not traditionally been used for imaging

soft tissue, improvements in resolution and image quality were compared to [21]. In [21], the applied beam energy and beam current were 140 kV and approximately 250 µA, respectively. Exposure time for each frame was 500 ms and no copper filter was used. All other settings in Table I were the same in as in [21].

Image resolution was directly influenced by distance to the detector. In [21], the entire FSU including the full vertebral bodies were captured in the image. For the current study, because the IVD was the primary focus, it was only necessary for images to include the IVD and adjacent endplates to capture potential endplate injury after applied loading. By maximising the ROI space with the IVD and endplates, the resulting image resolutions increased from approximately 10–12.5 voxels/mm (80–100 µm voxel size) in [21], to 22–29 voxels/mm (35-45 µm voxel size). These ranges reflect an increase in resolution of 76–190% compared to [21] and reflect over an order of magnitude higher resolutions compared to standard clinical CTs at approximately 0.625 – 1 mm pixel size.

Increasing the image quality involved the addition of a 0.125 mm copper filter which allowed for increasing the power (product of voltage and current) and increasing the scan time per projection. With the increased resolution and increased scan time, minimising movement became critical for image quality, as any motion greatly blurred the image. The additional techniques applied to this study that were not present in [21], including the customised mould and insulated container with dry ice, which helped to compensate for the higher sensitivity to movement. These measures were applied to the current study after preliminary imaging revealed significant blurring due to specimen thawing with the increased resolution and exposure time per frame. The tradeoffs in the current settings compared to [21] were an increase in designated scan time by approximately 30 minutes, and the loss of capturing the full adjacent vertebral bodies.

Figure 4 shows the enhanced image quality and resolution from the current porcine study (Fig. 4C) compared to prior microCT imaging of a porcine disc from [21] (Fig. 4B) and to *ex vivo* clinical CT imaging of a human intervertebral disc (Fig. 4A). Annulus fibers (Fig. 4D–F) for each imaging technique highlight the visual differences between the three. Individual lamellae are clearly resolved in the current study (Fig. 4F).

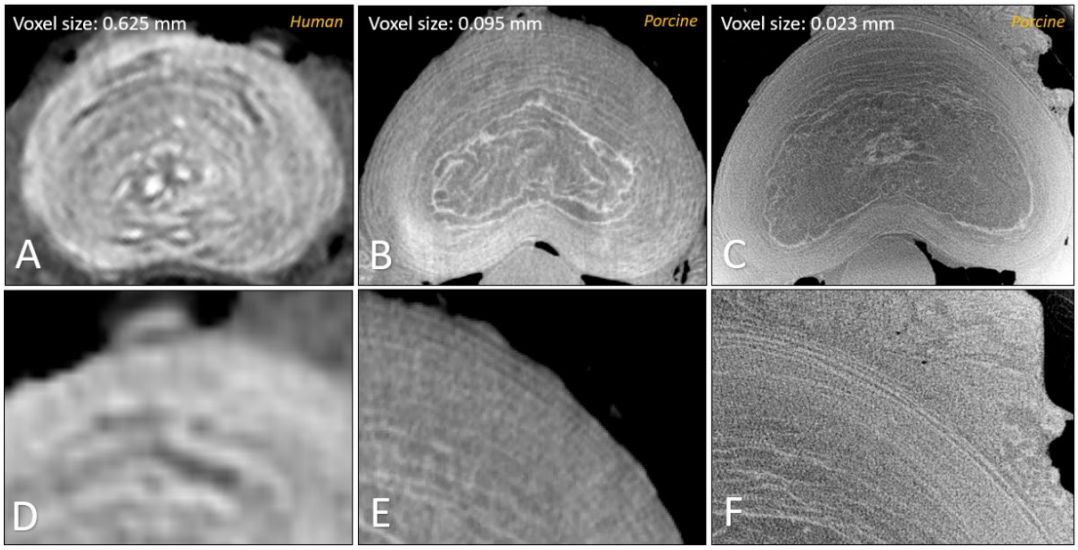

Fig. 4. (A) Clinical CT of *ex vivo* human lumbar IVD at 0.625 mm voxel size, (B) microCT of *ex vivo* porcine lumbar IVD in [21] at 0.095 mm voxel size, (C) microCT of *ex vivo* porcine lumbar IVD in Test 8 pre-test imaging from the current study at 0.023 mm voxel size. D-F show the annulus fibers for each technique.

There was a practical limit to minimising the voxel size. During post-testing imaging for two tests (Test 4, Test 6), the FSU was positioned too close to the detector, which resulted in overexposed imaging on the edges of the disc (Fig. 5A). Based on the other tests, a margin of 7–10 mm from the ROI to the edge of the frame was required to avoid overexposure on imaging (Fig. 5B). Therefore, the resolutions produced in these scans using this particular microCT model represent the practical maximum resolution of capturing a porcine disc due to its physical size. Subsequently, these two tests could not be properly analysed for the second part of the study. Additionally, an equipment issue with the freezer used between testing and post-test imaging for Test 8 resulted in premature thawing and large areas of substantial dehydration (appearing as large black voids), so Test 8 was also not analysed for the second part of the study. However, the loading exposure for this test was well outside of the 95% confidence interval for endplate fracture risk. This equipment issue also mildly affected Test 2 in outer left anterior annulus tissue. As the affected tissue was minimal in Test 2, the rest of the unaffected tissue was

analysed. The dehydrated area was indicated by the pink highlighted area in post-test imaging (Fig. 7C).

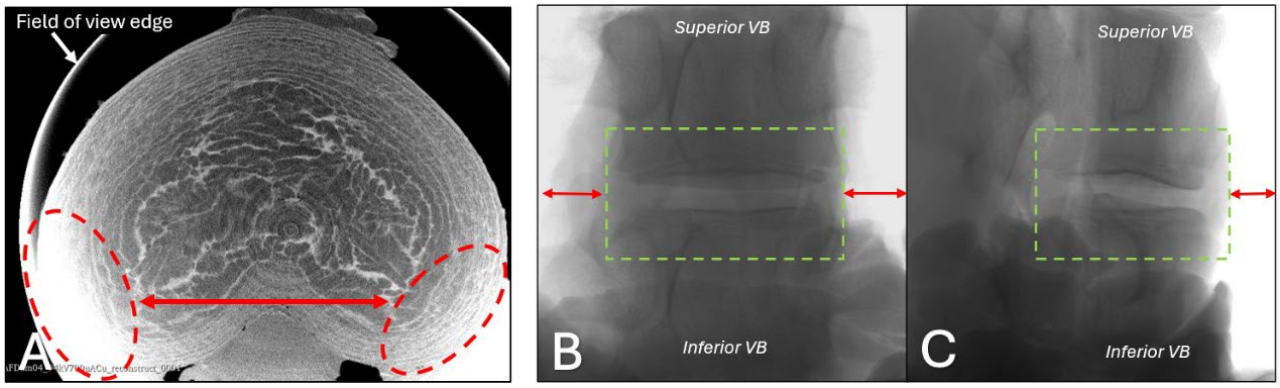

Fig. 5. (A) Overexposed outer edges of the disc in Test 6 due to positioning the FSU too closely to the detector. (B) Frontal and (C) sagittal x-ray views of the FSU pre-scan showing the recommended 7–10 mm margin (red arrows) between the ROI and edge of the frame.

Repeated Loading

The secondary objective of this study was to use this improved high-resolution imaging to capture changes in the porcine IVD subject to repeated flexion-compression just prior to endplate failure. All loading durations for the experimental tests were below the 50% endplate fracture threshold, developed in [21], for the applied peak compressive stress of 2.75 MPa (Fig. 6) [21]. Endplates were captured in pre- and post-test imaging (demonstrated in Fig. 5) to detect possible endplate failures due to applied loading, which would present as disruptions in the trabecular grain boundaries clearly resolved with the microCT. Post-test imaging confirmed there were no resulting endplate fractures for all control and test specimens. Test 1 and Test 2 were loaded for approximately one hour and 45 minutes, respectively, which were below the 50% EP fracture risk but within the 95% confidence interval. Test 5 was loaded for approximately 15 minutes, which was just outside of the 95% confidence interval for this applied stress. The remainder of the discussion will focus on these three tests that were just below the endplate injury threshold to discuss potential pre-injury morphology in the IVD. These tests will be referred to hereafter as the 'pre-fracture' tests. Final maximum strains and loading durations for each experimental test are shown in Table II.

TABLE II

SPECIMEN CHARACTERISTICS, RESULTING MAXIMUM STRAIN, AND TOTAL LOADING DURATIONS FOR ALL TESTS

	Pig No. and Mass	Spinal Level	Avg EP Area (mm^2)	Avg Initial EP-EP Height (mm)	Max EP-EP Strain (%)	Load Duration (hh:mm:ss)	Cycle Count
Test 1	1 (80 kg)	TX-L1	545	9.14	46.4%	01:03:38	3818
Test 2	2 (65 kg)	L2-L3	563	10.00	40.0%	00:44:31	2671
Test 3	6 (48 kg)	L5-L6	534	8.67	38.0%	00:04:50	290
Test 4	5 (76 kg)	L5-L6	646	9.44	35.4%	00:05:42	342
Test 5	3 (41 kg)	L3-L4	368	8.43	33.0%	00:14:39	879
Test 6	4 (76 kg)	L1-L2	643	10.20	30.0%	00:13:45	825
Test 7	4 (76 kg)	L3-L4	642	9.80	25.0%	00:01:32	92
Test 8	7 (44 kg)	L1-L2	414	8.20	20.0%	00:03:13	193
Test 9	8 (40 kg)	L5-L6	420	7.87	15.0%	00:00:20	20
Control 1	9 (80 kg)	L1-L2	596	10.05	0.0%	00:00:00	0

The current study did not quantify differences between pre- and post-testing images as the main objective was largely focused on capturing the IVD constituents and then capturing how these constituents are positioned prior to and after loading. Future work in characterising these observations in terms of specific tissue damage or reversible tissue changes, as well as quantifying these observations, would be incredibly valuable for statistically analysing the relationship between applied loading and injury risk. Pre- and post-test IVD images for the control and pre-fracture tests are shown in Fig. 7.

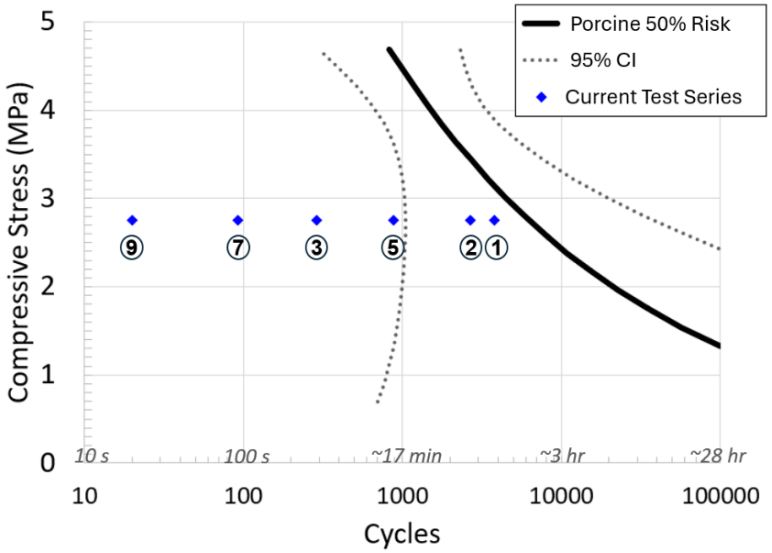

Fig. 6. Applied stress and duration exposures for test specimens (blue diamonds) overlayed with the 50% porcine endplate fracture risk (black line) and 95% confidence intervals (black dotted line) exposed to the repeated flexion-compression loading profile from Morino *et al*. [21].

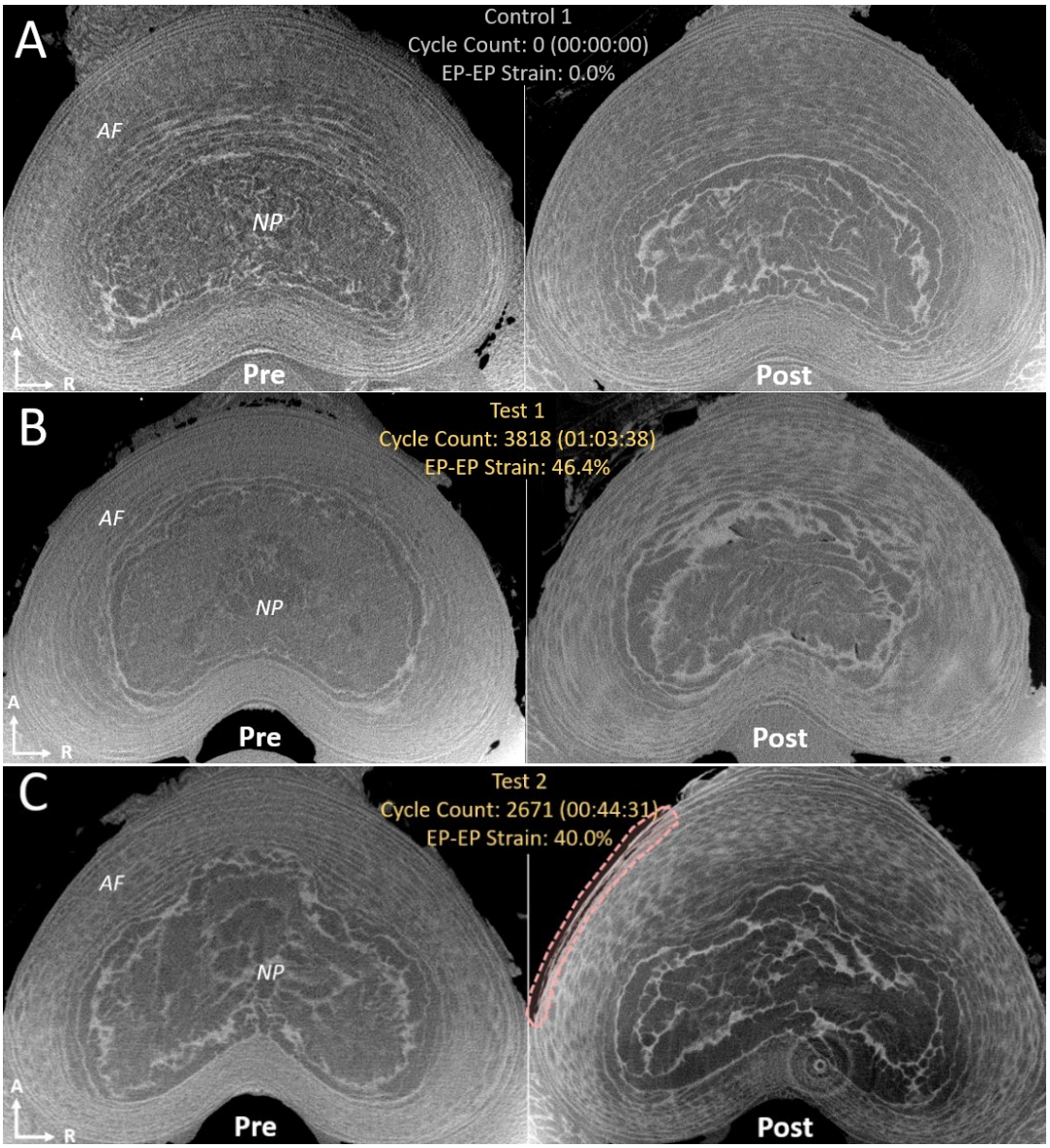

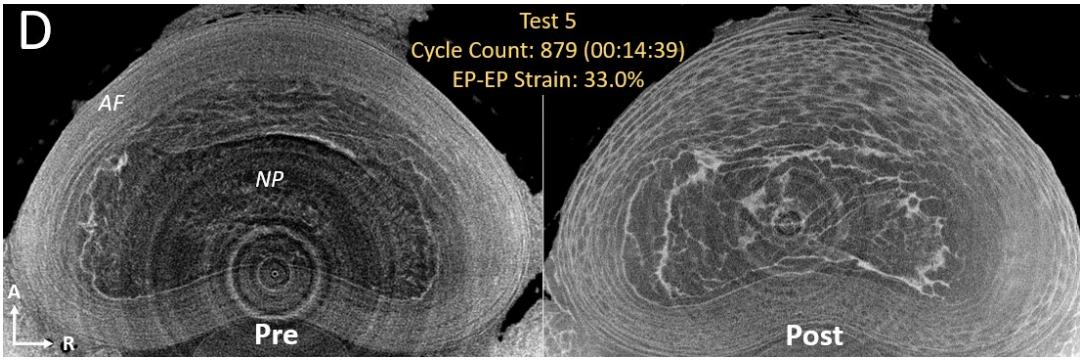

Fig. 7. Pre- and post-test axial images of IVDs for the control (A) and pre-fracture tests (B, C, D). Orientation axes denote anatomical anterior, 'A,' and right, 'R'. Pink highlighted area in (C) post-test indicates the area that was not considered for comparison due to premature thawing and dehydration.

IV. DISCUSSION

Imaging

Historically, microCT imaging has been used for non-destructive, high-resolution imaging of dense materials like bone or metal that have high x-ray attenuation. While other studies have used contrast agents that increase x-ray attenuation to improve soft tissue imaging, this offsets some of the advantages of microCT imaging as the effect of contrast agents on tissue microstructure is unknown [22-23]. In this study, microCT was used to improve direct imaging of the soft tissue within the IVD without intrusive measures.

The main efforts to increase image quality and resolution for this study involved utilising a copper filter, increasing power, minimising the voxel size, minmising specimen movement, and increasing the exposure time. To minimise voxel size, the disc and adjacent endplates were maximised in the field of view, often cutting off the posterior elements, transverse processes, and distal ends of the vertebral bodies. However, if any tissue of interest was too close to the edge of the field of view, this tissue was overexposed.

The scan times for this test series took approximately 94 minutes, substantially longer than clinical CT scan times, which only involve approximately 10 minutes of dedicated scan time. The scan time, a product of number of projections, frames per projection, and exposure time, is positively correlated with image quality. In theory, any of these factors accounting for scan time can be increased to improve the image quality. However, increased acquisition times increase the sensitivity to movement, resulting in greater blurring effects. Ring artifacts are visible in some of the microCT images, appearing as superimposed concentric lines in the reconstructed axial views. The minimise ring artifacts option was not applied to these images because the Gaussian filtering associated with this function causes blurring [26], which was counterproductive to the main objective.

The imaging objective for this study was principally to improve microCT imaging of the IVD. Dedicated optimisation of the microCT settings and procedures regarding optimal voltage, filtration, exposure time and other parameters would be valuable future work for potential further improvements. However, the imaging and resolution achieved in this study demonstrated the utility of this non-destructive imaging tool on soft tissue, which has not historically been used for soft tissue. In recent years, Disney *et al.* [27] found success imaging the IVD and its constituents non-invasively using synchrotron microCT and achieved higher resolutions than that of the current study. The current study presents a methodology using a more broadly accessible imaging modality, which is uniquely valuable for future adoption and utility for various soft tissue imaging goals. This novel imaging technique is uniquely useful for studying the changes in both the NP and AF when exposed to any kind of external loading. Individual annulus lamellae were distinguishable as well as non-water components that make up the NP. The non-destructive nature of this technique allows for capturing both incipient tissue failure and damage propagation within the IVD, both of which are essential to understanding pain-inducing injury in the low back.

While standard MRI imaging is limited, with relatively lower resolutions, ultra-high-field MRI has demonstrated increased image resolution and quality for IVD imaging. In recent years, Tavana *et al*. [28] utilised ultra-high-field MRI to image IVD constituents at in-plane resolutions of 90 microns with relatively short scan times (~17 minutes), although slice thickness using this technique was larger (~800 microns), limiting 3D reconstruction capabilities. In contrast, the current study used microCT to achieve isotropic resolutions around 30–40 microns, maintaining detail across all three dimensions, though with longer scan times (~90 minutes). The increasing accessibility of

microCT for research groups also offers an advantage for adopting the current technique to image IVD tissue.

Imaging techniques from the current study, synchrotron microCT [27], and ultra-high-field MRI [28], all come with their own limitations and advantages, but each of these modalities present exciting developments for capturing IVD behaviour and damage and potentially identifying key contributors of non-specific low back pain.

Initial IVD Observations and Future Work

Test 1 and Test 2 were loaded for a duration within the 95% confidence interval of EP failure, so it is likely the tissue morphology captured in these post-test images closely preceded EP fracture, while the exposure for Test 5 was just outside the 95% confidence interval. Two main observations were made when comparing post-test imaging of the pre-fracture tests to the respective pre-test images and control. In post-test imaging, the boundary between the NP and AF became less distinguishable from each other (Fig. 8) and the AF in post-test images appear to show separation between the lamellae (Fig. 9). There are various future directions to quantify these initial observations.

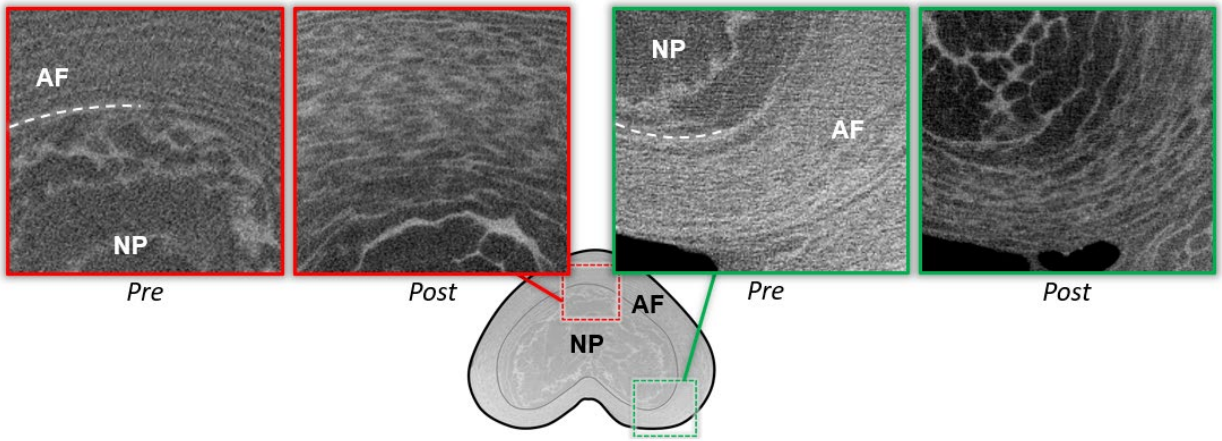

Fig. 8. Pre- and post-test images of IVD highlighting the NP-AF boundary changes in Test 2. The white dashed line in pre-test images shows the pre-test NP-AF boundary, which is less distinct in the IVD after loading. Pre- and post-test image boundaries are the same in dimension and location.

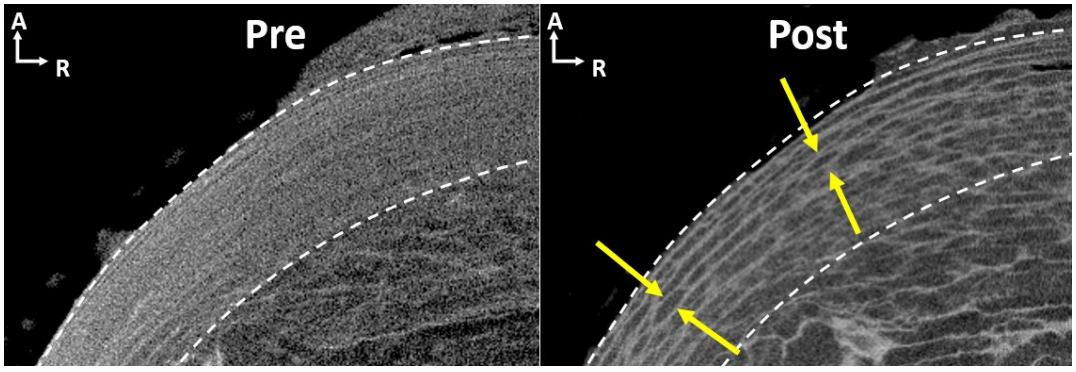

Fig. 9. Lamellae separations (yellow arrows) in annulus fibrosus (white dashed boundary) for Test 5 evident post-test compared to pre-test in anterior-left region.

The observations made from the NP-AF boundary in this study are likely due to water movement from and within the IVD, secondary to compressive loading, which has been well-documented and studied [19, 29]. Ghiss *et al.* [19] demonstrated with MRI how compression in the disc resulted in water movement from the NP into the outer AF with subsequent loading. This effect is accompanied by the seemingly smaller NP and more concentrated non-water components of the NP when compared to pre-test imaging (non-water components present as a lighter in colour compared to water in this imaging modality). This boundary effect was also identified in Sharabi *et al.* [29] where the microstructure of ovine IVDs was measured using ultrahigh field MRI. A clearer demarcation in the NP-AF transition zone of the younger discs (2 years old) was reported compared to the older discs (4-5 years old). The findings in this study along with the results published in [29] indicate this effect may be influenced by cumulative loading in the spine over time. However, the non-water NP components in the Control images do also appear affected, so the environmental conditions are likely contributing as well to an unclear extent. Other

studies have measured the NP dimensions manually (e.g., [28]), however, the effect of the NP-AF boundary being less distinguishable in post-test imaging made it difficult to manually measure changes in NP cross-sectional area objectively in the current study. Quantifying the NP volume, NP cross-sectional area, and the signal intensity for water would elucidate how water moved throughout the disc due to the repeated loading and how water loss is associated with subsequent injury. Future analysis of the sagittal and coronal images with respect to the NP-AF boundary geometric characteristics should also be compared to Tavana *et al.* [28] that found NP-AF boundary curvature to be significantly different between degenerate and non-degenerate IVDs.

Some of the most dramatic changes captured with the microCT imaging method in this study occurred in the AF. Also likely influenced by water flow out of the NP, the images capture the individual lamellae separating from each other, where they were tightly bound pre-loading (Fig. 9). Lamellae separation was captured with high-resolution images for the three pre-fracture tests anteriorly, laterally, and posteriorly. Next steps for quantifying this observation include measuring this distance between fibers, and fiber orientation pre- and post-loading.

Without quantifying these observations, it is unclear to what extent these visual differences are due to the repeated loading, the environmental conditions, or even the process of freezing, thawing, and re-freezing. Various pathways for quantifying these observations are noted above. Ideally, investigating potential relationships between these quantities (e.g., change in distance between fibers, NP water loss) and loading exposure could lead to identifying key characteristics in the disc just prior to tissue failure.

The methodology presented in this study can aid in future initiatives for studying IVD behaviour as it relates to injury. This study presents initial tissue observations in IVD tissue due to loading, but it is unclear how these tissue changes are affected after rest, rehydration, and eventual subsequent loading. Capturing the IVD at several timepoints during representative diurnal loading patterns would elucidate if these observations are reversible or if the observations represent microscale damage that accumulates over time until clinically detectable injury occurs. Additionally, a critical next step for this work is pairing this nondestructive imaging with validated tissue failure identification methodologies such as histology, so observations made with microCT imaging can eventually exclusively identify tissue failure in the disc.

Real-world Relevancy

Importantly, the applied stress in this study was substantially larger than diurnal loads, but the theory of accelerated life analysis suggests that injury risk at high stress and short durations is similar to that of lower stress exposures over longer durations [21]. Thus, results observed in this study are interpreted as tissue changes that could also occur at much lower stresses over much longer durations (i.e. years).

Currently, the only practical application for this imaging methodology is with *ex vivo* specimens. A primary limitation preventing clinical use of microCT is radiation exposure, which is linked to an increased risk of developing cancer [4]. Cadaver specimens were exposed to high power radiation over long exposures, resulting in high-resolution images. Another important aspect of this methodology is the high sensitivity to movement that necessitated the techniques for keeping the specimens frozen and rigid, which presents an inevitable practicality issue even if future clinical CT technology allowed for higher resolutions. The imaging techniques and methodology demonstrated in the current study are most useful for investigating injury in *ex vivo* specimens where incipient microscale tissue changes can be captured.

Tissue changes captured in this study presented microscale IVD changes, particularly in the annulus fibrosus, prior to any bony injury, that could be relevant to pain in the low back due to the innervation of outer annulus lamellae. If future studies can eventually use this noninvasive, high-resolution imaging to detect microscale tissue failure in the AF prior to clinically visible injury, this could have significant implications for nonspecific LBP etiology. Even if microCT techniques cannot directly translate into clinical CT, experimentally capturing damage to the IVD prior to clinically visible injury would be critical for developing specific and efficacious treatment as well as understanding occupational risk that would directly inform injury prevention measures.

Pig Model and Study Limitations

While the primary limitation for animal models is due to interspecies differences, in this case, using a porcine model rather than human tissue was particularly advantageous. Young, healthy, human cadaver donors are scarce, therefore most studies using human cadaver tissue are limited to older donors. Using young porcine specimens allows for a level of experimental control that would be difficult with older human cadaver subjects. Further, gel-like porcine NP is similar to the NP in children in terms of water content [30]. Porcine NP is made up

of approximately 88% water, which makes the NP and AF more distinguishable from one another [31]. As we age, the NP becomes less hydrated and more fibrous, consequently making it less distinguishable from the AF [30]. The pre-test porcine IVDs have a clear NP-AF boundary, so controlled comparisons can be made pre-test to post-test. While porcine tissue was particularly advantageous for this study, interspecies differences could certainly influence how these results would differ in human tissue. Further studies are needed to determine how these results may relate to *ex vivo* and *in vivo* human tissue.

Phantoms were excluded from imaging and ring artifacts were not filtered out to maximise the image resolution. Density calibrations from the phantoms would have been useful for potentially measuring water in between pre-test and post-test, as well as standardising the greyscale values in all images. The presence of ring artifacts obscured lamellae in the posterior AF at times. These were tolerable limitations for minimising voxel size and maintaining image quality, the primary study objective.

V. CONCLUSION

The primary objective of this study was to improve microCT imaging of soft tissue, compared to other published microCT imaging studies. By decreasing the voxel size, minimising specimen movement, and increasing scan exposure time, microscale components of porcine intervertebral disc were visually distinct, including individual lamellae within the annulus fibrosus and non-water components of the NP. Resolutions of 22–29 voxels/mm were produced with the present methodology which demonstrates substantial improvement from images in the previous study [21] producing resolutions of 10–12.5 voxels/mm and at least an order of magnitude better than clinical CT with resolutions at 1.6 pixels/mm. The second objective was to use this novel imaging technique to capture intervertebral disc tissue changes just prior to endplate failure in porcine lumbar FSUs exposed to repeated flexion-compression. Three test specimens loaded near the endplate fracture threshold showed changes in the AF and NP of the IVD without experiencing endplate failure. In these specimens, initial observations indicated the boundary between the nucleus pulposus and annulus fibrosus became less distinct, and the annulus fibrosus showed separation between lamellae. Future work is needed to quantify these initial tissue observations prior to injury and to establish how pre-injury observations are associated with reversible loading behaviour or microscale damage. Tissue changes captured with the high-resolution imaging in this study could have significant implications for understanding low-level injuries contributing to low back pain that would be impossible to detect with current clinical imaging capabilities. This non-destructive imaging methodology should be used in future lumbar spine investigations to capture and determine incipient tissue failure due to various external loading regimes.

VI. ACKNOWLEDGEMENTS

The authors gratefully acknowledge funding from the Office of Naval Research and US Naval Air Systems Command – Patuxent River through MTEC (Southwest Research Institute-PI).

VII. REFERENCES

[1] Maher, C., Underwood, M., Buchbinder, R. (2017) Non-specific low back pain. *The Lancet*, **389**(10070): pp.736–747.

[2] Fatoye, F., Gebrye, T., Odeyemi, I. (2019) Real-world incidence and prevalence of low back pain using routinely collected data. *Rheumatology International*, **39**: pp. 619–626.

[3] Jarvik, J. G., Hollingworth, W., *et al*. (2003) Rapid magnetic resonance imaging vs radiographs for patients with low back pain: A randomized controlled trial. *The Journal of the American Medical Association*, **289** (21): pp. 2810 Jama 2818.

[4] Chou, R., Qaseem, A., Owens, D. K., Shekelle, P. (2011) Diagnostic imaging for low back pain: Advice for high-value health care from the American College of Physicians. *Annals of Internal Medicine*, **154**(3): pp. 181–189.

[5] Jenkins, H., Downie MChir, A., *et al.* (2018) Imaging for low back pain: is clinical use consistent with guidelines? A systematic review and meta-analysis. *The Spine Journal*, **18**(12): pp. 2266–2277.

[6] Whatley, B. R., Wen, X. (2012) Intervertebral disc (IVD): Structure, degeneration, repair and regeneration. *Materials Science and Engineering: C*, **32**(2): pp. 61–77.

[7] Cyril, D., Giugni, A., *et al.* (2022) Elastic fibers in the intervertebral disc: From form to function and toward regeneration. *International Journal of Molecular Sciences*, **23**(16): p. 8931.

[8] Cassidy, J., Hiltner, A., Baer, E. (1989) Hierarchical structure of the intervertebral disc. *Connective Tissue Research*, **23**(1): pp. 75–88.
[9] Sun, Z., Sun, Y., Mi, C. (2023) Comprehensive modeling of annulus fibrosus: From biphasic refined characterization to damage accumulation under viscous loading. *Acta Biomaterialia*, **174**(15): pp. 228–244.
[10] Adams, M. A., Hutton, W. (1985) Gradual disc prolapse. *Spine*, **10**(6): pp. 524–531.
[11] Gregory, D., Bae, W., Sah, R., Masuda, K. (2012) Anular delamination strength of human lumbar intervertebral disc. *European Spine Journal*, **21**: pp. 1716–1723.
[12] Ghezelbash, F., Schmidt, H., Shirazi-Adl, A., El-Rich, M. (2020) Internal load-sharing in the human passive lumbar spine: Review of in vitro and finite element model studies. *Journal of Biomechanics*, **102**: p. 109441.
[13] García-Cosamalón, J., Del Valle, M., *et al.* (2010) Intervertebral disc, sensory nerves and neurotrophins: Who is who in discogenic pain? *Journal of Anatomy*, **217**(1): pp. 1–15.
[14] Binch, A. L., Cole, A. A., *et al*. (2015) Nerves are more abundant than blood vessels in the degenerate human intervertebral disc. *Arthritis Research & Therapy*, **17**(370).
[15] Groh, A., Fournier, D., Battié, M., Séguin, C. (2021) Innervation of the human intervertebral disc: A scoping review. *Pain Medicine*, **22**(6): pp. 1281–1304.
[16] Veres, S. P., Robertson, P. A., Broom, N. D. (2009) The morphology of acute disc herniation: A clinically relevant model defining the role of flexion. *Spine*, **34**(21): pp. 2288–2296.
[17] Zhang, Y., Drapeau, S., *et al*. (2011) Histological features of the degenerating intervertebral disc in a goat disc-injury model. *Spine*, **36**(19): pp. 1519–1527.
[18] Wade, K., Robertson, P., Thambyah, A., Broom, N. (2014) How healthy discs herniate: A biomechanical and microstructural study investigating the combined effects of compression rate and flexion. *Spine*, **39**(13): pp. 1018–1028.
[19] Ghiss, M., Giannesini, B., Tropiano, P., Tourki, Z., Boiron, O. (2016) Quantitative mri water content mapping of porcine intervertebral disc during uniaxial compression. *Computer Methods in Biomechanics and Biomedical Engineering*, **19**(10): pp. 1079–1088.
[20] Wijayathunga, V. N., Tanner, S. F., Ridgway, J. P., Wilcox, R. K. (2019) An in vitro study of the intervertebral disc structure using 3 T magnetic resonance imaging. *Spine*, **44**(11): pp. 793–800.
[21] Morino, C., Schmidt, A., *et al*. (2024) Human and porcine lumbar endplate injury risk in repeated flexion-compression. *Annals of Biomedical Engineering*, **54**: pp. 1009–1022.
[22] Keklikoglou, K., Arvanitidis, C., *et al*. (2021) Micro-CT for biological and biomedical studies: A comparison of imaging techniques. *Journal of Imaging*, **7**(9): p. 172.
[23] Naveh, G., Brumfeld, V., Dean, M., Shahar, R., Weiner, S. (2014) Direct micro-ct imaging of non-mineralized connective tissues at high resolution. *Connective Tissue Research*, **55**(1): pp. 52–60.
[24] Ren, L., Ghani, M., *et al.* (2016) The impact of spectral filtration on image quality in micro-ct system. *Journal of Applied Clinical Medical Physics*, **17**(1): pp. 301–315.
[25] Bass, C., Salzar, R., Ziemba, Z., Lucas, S., Peterson, R. (2005) The modeling and measurement of humans in high speed planing boats under repeated vertical impacts. *Proceedings of the IRCOBI Conference*, 2005, Prague, Czech Republic.
[26] Eldib, M. E., Hegazy, M., *et al*. (2017) A ring artifact correction method: Validation by micro-ct imaging with flat-panel detectors and a 2d photon-counting detector. *Sensors*, **17**(2): p. 269.
[27] Disney, C. M., Eckersley, A., *et al*. (2019) Synchrotron tomography of intervertebral disc deformation quantified by digital volume correlation reveals microstructural influence on strain patterns. *Acta Biomaterialia*, **92**: pp. 290–304.
[28] Tavana, S., Shek, C., Rahman, T., Baxan, N., Newell, N. (2024) The influence of geometry on intervertebral disc stiffness. *Journal of Biomechanics*, **163**: p. 111915.
[29] Sharabi, M., Wade, K. R., *et al.* (2018) Three-dimensional microstructural reconstruction of the ovine intervertebral disc using ultrahigh field MRI. *The Spine Journal*, **18:** pp. 2119–2127.
[30] Iatridis, J., Weidenbaum, M., Setton, L., Mow, V. (1996) Is the nucleus pulposus a solid or a fluid? Mechanical behaviors of the nucleus pulposus of the human intervertebral disc. *Spine*, **21**(10): pp. 1174–1184.
[31] Morino, C., Kait, J., Bass, C. R. (2024) Hydration State Throughout Porcine Lumbar Intervertebral Discs: Comparing Fresh and Frozen-Thawed Specimens. *Annals of Biomedical Engineering*, **54**: pp. 1068–1075.